AIAA Aviation
22-26 June 2015, Dallas, TX
AIAA Atmospheric Flight Mechanics Conference

Rapid, Robust Trajectory Design Using Indirect Optimization Methods

Michael J. Grant*
Purdue University, West Lafayette, IN, 47906
Michael A. Bolender†
Air Force Research Laboratory, Wright-Patterson Air Force Base, OH, 45433

An efficient methodology is created to formulate robust trajectory design problems within an indirect optimization framework. An augmented cost functional is used to capture the worst case scenario associated with each modeled dispersion. This approach eliminates the need to propagate statistical information, thereby minimizing the dimension of the design problem. The proposed methodology enables robustness considerations to be directly incorporated into the optimization problem in which the mathematical information associated with indirect methods is used to provide explicit interaction information among nominal and dispersed trajectories. Examples illustrate the ability to construct highly coupled, complex solutions that capture all of the robustness considerations of interest to the designer. This approach enables the rapid construction of families of solutions that trade performance and robustness based on designer preference.

Nomenclature

$\mathbf{u}$	control vector	m	mass, kg
$\mathbf{x}$	state vector	N	number of states
C_D	drag coefficient	R	robustness metric
C_L	lift coefficient	r	radial magnitude, m
D	dispersion gradient (mixed units) or drag force magnitude, N	v	velocity, m/s
		w	multiobjective weighting factor
k	index of state vector	x	x-coordinate, m
L	lift force magnitude, N	y	y-coordinate, m
M	number of shadow vehicles		

γ	relative flight-path angle, rad	μ	gravitational parameter, m^3/s^2
$\mathbf{\Delta}$	vector of worst case dispersion magnitudes captured by shadow vehicle	θ	wire angle or downrange angle, rad

I. Introduction

Traditionally, conceptual hypersonic design is performed using direct optimization methods.[1–6] Prior research by Grant has demonstrated that the historical optimal control challenges associated with indirect optimization methods can be largely overcome to perform hypersonic mission design. The creation of the necessary conditions of optimality is performed in a completely automated fashion by leveraging modern symbolic computational tools such as Mathematica. By formulating the optimality conditions in a generic

*Assistant Professor, School of Aeronautics and Astronautics, AIAA Senior Member.
†Senior Aerospace Engineer, AIAA Associate Fellow.

fashion, the application of appropriate boundary conditions associated with various constraint arc sequences can be dynamically enforced by employing a continuation process.[7,8] Additionally, by solving a sequence of progressively difficult optimization problems via continuation, it is possible to create complex optimal trajectory solutions that fully satisfy the necessary conditions of optimality without supplying a good initial guess to the complex solution.

As an example, an indirect solution can be easily constructed for a short, unconstrained, minimum heat load trajectory as shown in Fig. 1. While this trajectory is of little interest to the designer, the optimal solution can be easily and rapidly evolved to the desired optimal solution using indirect optimization methods. This is accomplished by first extending the trajectory to match the desired initial and terminal conditions as shown in Fig. 2. After this process is completed, heat rate and g-loading constraints can be introduced and incrementally reduced to the desired value as shown in Figs. 3 and 4, resulting in a fully constrained, minimum heat load trajectory. In this optimal control framework, the derivation of the necessary conditions of optimality, application of appropriate multi-point boundary conditions throughout the continuation process, and management of the continuation parameters is performed in an automated manner that is transparent to the designer. This automation has greatly reduced the historical burden of using optimal control theory to perform rapid mission design. In this example and in the examples provided in this investigation, Mathematica is used to develop the necessary conditions of optimality, and Matlab scripts are automatically generated with this information. The scripts are then automatically autocoded to C, and the resulting boundary value problems are solved using Matlab's *bvp4c*.

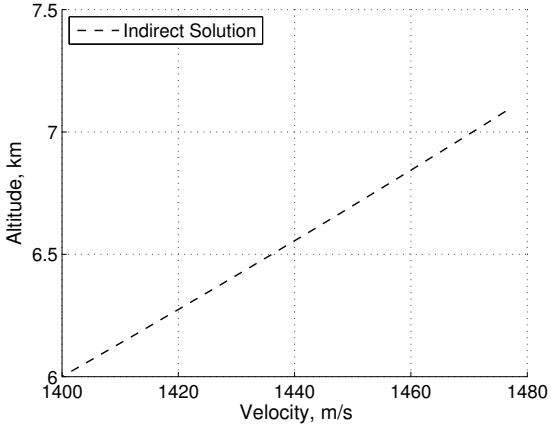

Figure 1: Initial indirect solution.

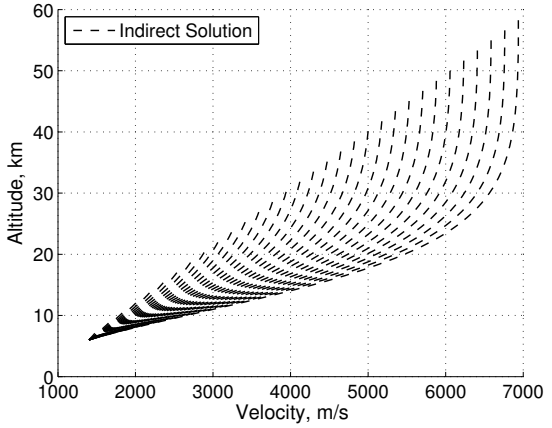

Figure 2: Trajectories from unconstrained continuation.

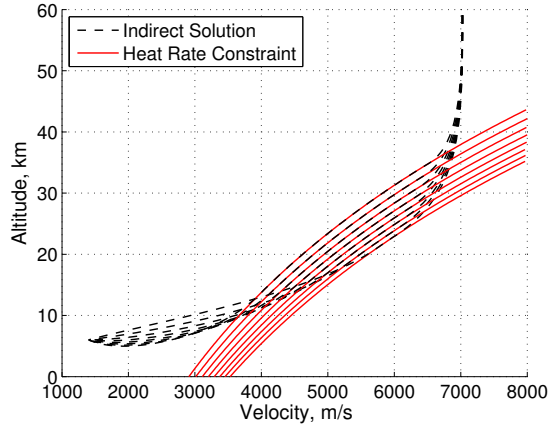

Figure 3: Trajectories from continuation of heat rate constraint.

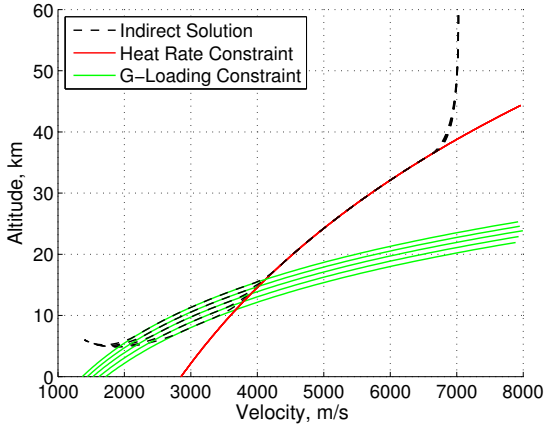

Figure 4: Trajectories from continuation of g-loading constraint.

To perform robust trajectory design, the objective function traditionally associated with nominal vehicle performance is often augmented to include robustness considerations. Common applications include the assessment of terminal state errors due to dispersions in the initial state and other parameters.[9–11] To assess dispersed performance, statistical information is often propagated via a covariance analysis. By assuming that dispersions retain a Gaussian form along the trajectory, the dynamics of the covariance matrices are propagated and interrogated to provide expected probability density functions at the terminal point of the trajectory. However, due the rather large increase in dimensionality associated with the inclusion of covariance matrix elements as states, the covariance dynamics are often carried forward separately such that they are propagated only during evaluation of the cost function.[9,10] As such, the propagation of covariance information is used as an efficient substitute for Monte Carlo analyses to support trajectory design. Since the states are only of the nominal trajectory, path constraints can only be applied to the nominal trajectory. Therefore, trajectories cannot be constructed that are also robust to path constraints. Alternatively, generalized polynomial chaos theory has been used to efficiently propagate statistical moment information associated with uncertainties. While this has been shown to be computationally efficient when propagating high order moment information, previous work has demonstrated that no dimension advantages exist for the common low order mean and variance propagations.[11]

The prior techniques enable the propagation of statistical information within evaluations of the cost function without the need to perform computationally intensive Monte Carlo simulations. As an alternative, stress cases can be used to capture the worst-on-worst set of dispersions that would be expected from Monte Carlo simulations.[12,13] These stress cases are created by the trajectory designer by noting that in many robust trajectory design applications, there is little interest in the probability density functions. Instead, trajectories are often designed to the worst case scenarios. In all of these robust trajectory design approaches, the dispersed performance of a candidate robust trajectory is evaluated as a function evaluation within direct optimization techniques. While all of these approaches enable trajectory shaping to provide robust solutions, the techniques do not leverage all of the mathematical information that exists to create robust trajectories. The following investigation highlights a robust trajectory design methodology that efficiently captures the trade in nominal and robust performance in a manner that is generally of most interest to conceptual hypersonic designers through the use of indirect optimization methods.

II. Rapid, Robust Trajectory Design Methodology

The use of indirect optimization methods allows the construction of an efficient methodology that is capable of capturing the robust trajectory features of interest during design. The following brachistochrone example is used to describe the methodology as well as illustrate the rapid, high quality solutions obtained using this approach. Note that in the direct methods described in Section I, an assumption is often made that uncertainties retain a Gaussian form along the trajectory. In the proposed methodology, no assumption is made regarding the distribution of the uncertainties during trajectory propagation.

II.A. Brachistochrone Example

The classic brachistochrone problem consists of designing the shape of a wire between two fixed points that minimizes the time for a frictionless bead within a constant gravity field to slide from the upper to the lower endpoint.[14] The equations of motion for this problem are shown in Eqs. (1) - (3), where θ is the control that determines the local slope of the wire.

$$\dot{x} = v\cos\theta \tag{1}$$

$$\dot{y} = -v\sin\theta \tag{2}$$

$$\dot{v} = g\sin\theta \tag{3}$$

II.A.1. The Trade Between Nominal Performance and Robust Design

In this simple example, the nominal initial velocity of the bead is 1.0 m/s, and the minimum time solution constructed using indirect methods is shown in Fig. 5. However, the designer may also be interested in

designing a trajectory that is robust to errors in the terminal state due to uncertainties in the initial state. A robust solution due to a maximum initial velocity uncertainty of 0.9 m/s that minimizes errors in x_f is also shown in Fig. 5, where it is assumed that the bead is in constant contact with the wire. This example demonstrates the trade in performance (time) and robustness (terminal accuracy) that exists when designing trajectories, and Fig. 6 illustrates the intermediate solutions associated with this trade.

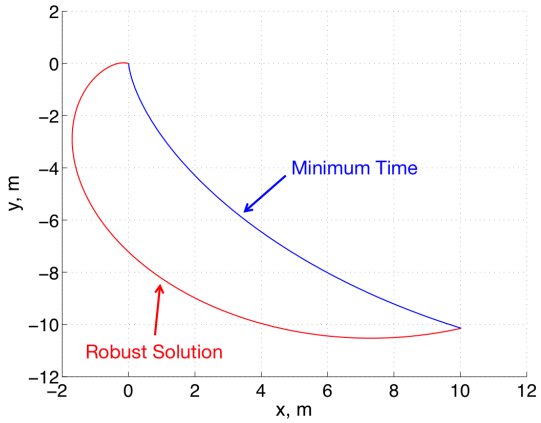

Figure 5: Optimally performing vs. robust brachistochrone trajectory.

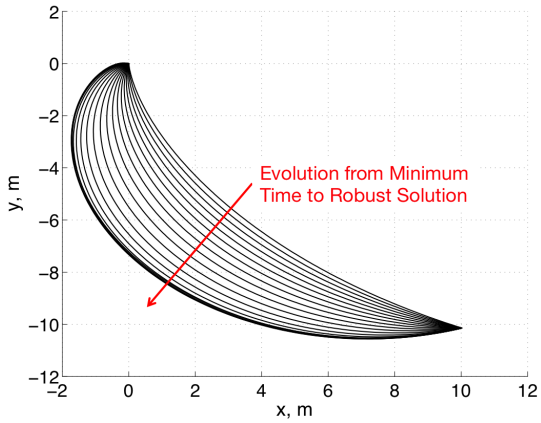

Figure 6: Transition between optimally performing and robust solutions.

It is possible to construct the robust solution by adding covariances matrix elements as states (as described in Refs. 9 and 10), thereby formulating an objective functional that minimizes the magnitude of the covariance matrix elements associated with x at the terminal point. For a significant number of uncertainties, this approach would greatly increase the dimensionality of the optimization problem. Furthermore, if a trajectory must be constructed that is also robust to path constraints, then the information within the covariance matrix must be repeatedly interrogated throughout the trajectory to determine dispersed performance. During conceptual design, the designer is often only concerned with the worst case dispersed trajectories. As such, the propagation of statistical information throughout the trajectory is not needed, as long as the worst case scenario(s) related to robustness are appropriately captured. The designer selects the worst case scenario that corresponds to the level of robustness desired (99^{th} percentile, 3σ, etc.). In the proposed methodology, these worst case scenarios are captured using "shadow vehicles" that are propagated alongside the physical vehicle (representing the nominal trajectory) according to the worst case dispersions.

II.A.2. The Use of Shadow Vehicles To Capture Worst Case Scenarios

As an example, consider the prior robustness and performance trade shown in Fig. 5. The minimum time solution corresponds to an optimization in performance alone, where robustness to errors in x_f due to initial velocity uncertainties is not considered. When propagating the worst case initial velocity uncertainty (represented by the path of Shadow Vehicle 1) as shown in Fig. 7 for the same time as the physical vehicle, a large error in x_f demonstrates that the trajectory of the physical vehicle is not robust in x_f to initial velocity uncertainties. Alternatively, Fig. 8 illustrates that the robust trajectory of the physical vehicle is insensitive to x_f errors due to initial velocity uncertainties as demonstrated by the worst case shadow vehicle trajectory. This is accomplished by optimizing the aggregated objective functional shown in Eq. (4), where w represents the relative weighting of importance between performance (minimum time) and robustness (small x_f error between the physical vehicle and worst case shadow vehicle).

$$J = (w)t_f + (1-w)(x_{f,\text{physical}} - x_{f,\text{shadow}})^2 \tag{4}$$

The initial state of the shadow vehicle is selected such that the trajectory of the shadow vehicle appropriately reflects the worst case scenario associated with a particular dispersion. This is accomplished by first noting the desired robustness metric as shown in Eq. (5) for the brachistochrone example. The dispersion gradient, $\nabla\mathbf{D}$, is calculated as shown in Eq. (6) to determine the direction in which the shadow vehicle should be placed relative to the physical vehicle, where $\mathbf{x_{f,physical}}$ represents the full state vector of the

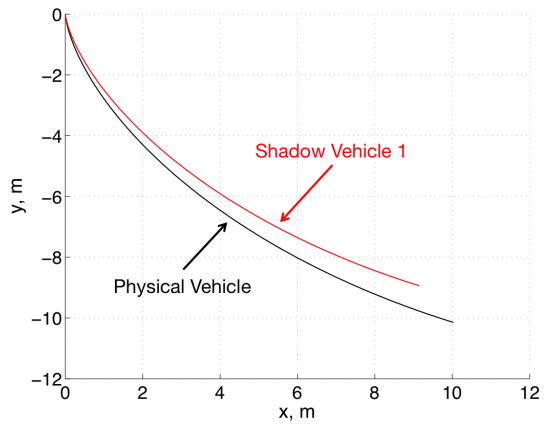

Figure 7: Nominal and shadow vehicle trajectories for minimum time case.

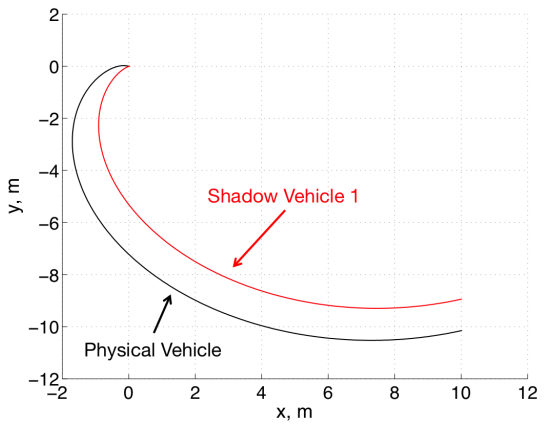

Figure 8: Nominal and shadow vehicle trajectories for x_f robustness case.

physical vehicle at the terminal point. This is accomplished by computing sensitivities associated with the nominal trajectory of the physical vehicle using the state transition matrix (STM), ϕ. Note that the dispersion gradient essentially describes the maximum adverse change in robustness (at the terminal point) due to changes in state at the initial point. While higher order state transition tensors could be used to capture nonlinear features of the dispersion gradient, the examples contained in this investigation only leverage the first order state transition matrix. Comparisons to Monte Carlo results indicate the sufficiency of neglecting higher order effects. Note that the use of the state transition matrix results in a large initial dimensional growth of the system. However, each additional dispersion results in a linear growth of dimensionality due to the inclusion of an additional shadow vehicle. Note that the elements of the state transition matrix are included as states to the indirect optimization problem. As such, each state transition matrix element has a corresponding costate, and the identity matrix is enforced as a boundary condition of the state transition matrix at the initial point of the trajectory.

$$R = (x_{f,\text{physical}} - x_{f,\text{shadow}})^2 \tag{5}$$

$$\nabla \mathbf{D} = \left(\frac{\partial R}{\partial \mathbf{x_{f,physical}}} \right)^T \phi(t_0, t_f) \tag{6}$$

After calculating the dispersion gradient, a constraint of the initial location of the shadow vehicle is enforced to place the shadow vehicle along the worst case direction from the physical (nominal) vehicle's initial state. Since the dispersion gradient is computed using the state transition matrix associated with the physical vehicle, the dispersion gradient shown in Eq. (6) describes the change in robustness due to changes in the initial state of the physical vehicle. As such, the worst case dispersion captured by the shadow vehicle would require an initial displacement from the physical vehicle in the direction opposite of the dispersion gradient as shown in the scalar Eq. (7) for the k^{th} state, where $\mathbf{\Delta}$ is a vector of the worst case dispersion magnitudes captured by the shadow vehicle. This initialization constraint ensures that during the optimization process, the shadow vehicle is always placed at the worst case location relative to the physical vehicle. This enables the trajectory of the physical vehicle to be altered during the design process while simultaneously ensuring that the shadow vehicle represents the corresponding worst case dispersion.

$$\mathbf{x_{0,shadow,k}} = \mathbf{x_{0,physical,k}} - \left(\frac{\nabla \mathbf{D_k}}{||\nabla \mathbf{D}||} \right) \cdot \mathbf{\Delta_k} \tag{7}$$

II.A.3. Mathematical Coupling Between Physical and Shadow Vehicles Using Indirect Methods

Unlike traditional design approaches that connect nominal and dispersed performance through function evaluations as described in Section I, the trajectories of the physical and shadow vehicles are deeply coupled

mathematically. As such, the trajectories of the physical and shadow vehicles are not independently optimized with only a loose coupling via the constraint in relative initial states as shown in Eq. (7). The physical and shadow vehicles are also coupled with the same control history, $\mathbf{u}$, as described by Eqs. (8) and (9), where $\mathbf{f}$ represents the equations of motion. To be robust to dispersions, the nominal trajectory of the physical vehicle must be constructed such that, in a worst case scenario, the same control history provides a robust solution in the presence of expected dispersions. As such, the control of the shadow vehicle cannot be independently optimized to provide improved performance in the presence of the worst case dispersion that the shadow vehicle represents. More importantly, when using indirect optimization methods derived from optimal control theory, the control history shared by both the physical and shadow vehicles is a function of the states and costates of both vehicles as well as of the sensitivities captured by the state transition matrix. This feature arises from the optimal control calculation shown in Eq. (10) for problems with a terminal point cost only, where H represents the Hamiltonian, λ represents the costate vector, $\mathbf{f_{STM}}$ represents the equations of motion of the state transition matrix elements, and $\mathbf{u_i}$ represents the i^{th} shared control. The explicit mathematical coupling between the physical and shadow vehicles enables the complex interactions associated with nominal performance (from the physical vehicle) and dispersed performance (from the shadow vehicle) to be captured in a high quality manner during the design process using indirect optimization methods.

$$\dot{\mathbf{x}}_{\mathbf{physical}} = \mathbf{f}(t, \mathbf{x}_{\mathbf{physical}}, \mathbf{u}) \tag{8}$$

$$\dot{\mathbf{x}}_{\mathbf{shadow}} = \mathbf{f}(t, \mathbf{x}_{\mathbf{shadow}}, \mathbf{u}) \tag{9}$$

$$\frac{\partial H}{\partial \mathbf{u_i}} = {\lambda_{\mathbf{physical}}}^T \cdot \frac{\partial \mathbf{f}(t, \mathbf{x}_{\mathbf{physical}}, \mathbf{u})}{\partial \mathbf{u_i}} + {\lambda_{\mathbf{shadow}}}^T \cdot \frac{\partial \mathbf{f}(t, \mathbf{x}_{\mathbf{shadow}}, \mathbf{u})}{\partial \mathbf{u_i}} + {\lambda_{\mathbf{STM}}}^T \cdot \frac{\partial \mathbf{f_{STM}}}{\partial \mathbf{u_i}} = 0 \tag{10}$$

II.A.4. Robust Design to Path Constraints

For each additional robustness consideration, a new shadow vehicle must be included in the optimization process. For path constraints in the brachistochrone problem, the worst case initial velocity (relative to the designed physical vehicle trajectory) is propagated using a second shadow vehicle as shown in Fig. 9. Since path constraints are often viewed as hard constraints, this shadow vehicle is enforced to not violate the path constraint. Note that in this case, the control (which is equivalent across the physical and two shadow vehicles) is influenced by the states and costates of the physical vehicle and both shadow vehicles such that the appropriate balance between performance and robustness is achieved. These complex interactions include the discontinuities of the costates of the second shadow vehicle due to the corner conditions at the entrance to the path constraint as shown in Figs. 10 and 11. As an example, consider a linear path constraint of the form shown in Eq. (11), where h determines the location of the constraint. The propagation of the additional shadow vehicle enables a sufficient push-off factor of the physical vehicle trajectory such that the constraint is not violated in the worst case scenario. Note, however, that this push-off factor is designed in a manner that also simultaneously provides a robust solution to errors in x_f. This additional path constraint reduces the performance of the physical vehicle such that the travel time is increased. This example demonstrates the feasibility of accounting for various robustness considerations within an indirect optimization framework. Additionally, the robustness considerations are addressed directly within the optimization problem by propagating additional shadow vehicles that capture the worst case scenarios of interest to the designer. This example highlights the ability to provide sufficient robustness

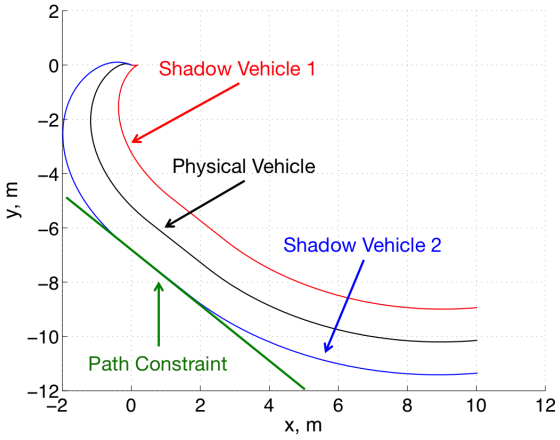

Figure 9: Robustness to path constraint.

to mid-flight considerations such as path constraints, a feature that is not readily available in many modern robust design methodologies.

$$0 > h - x_{\text{shadow}} \tan(45^o) - y_{\text{shadow}} \tag{11}$$

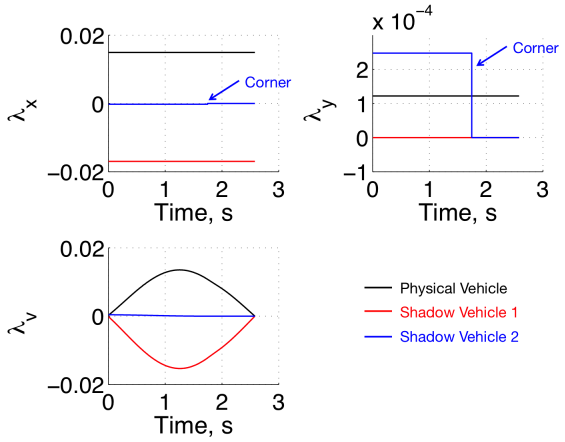

Figure 10: Costates of physical and shadow vehicles.

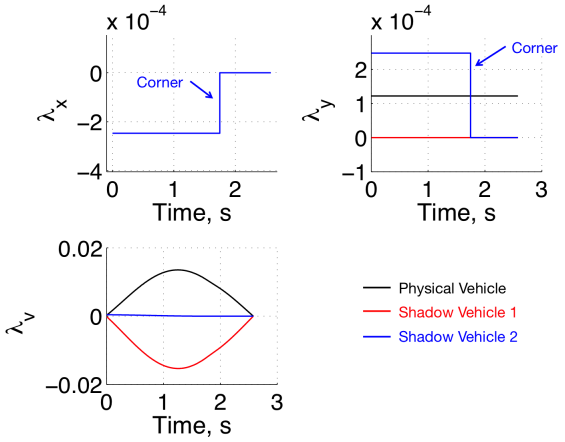

Figure 11: Zoomed in view of costates of physical and shadow vehicles.

It is important to note that the initial state of the second shadow vehicle is selected to provide the worst case dispersion associated with the potential violation of the path constraint. As such, the initial state of the shadow vehicle is calculated in a similar manner as shown in Eq. (7). Since the worst case scenario maximizes the potential violation of the path constraint, the robustness metric is formulated as simply the expression of the path constraint as shown in Eq. (12), where larger values imply greater violation of the constraint and t_1 corresponds to the time of the entrance to the path constraint. Since the robustness metric occurs at t_1 instead of t_f, the dispersion gradient leverages the state transition matrix at time t_1 as shown in Eq. (13). During the continuation process, path constraints are included as described in the planar hypersonic example in Fig. 3 of Section I. The indirect optimization framework is capable of automatically splitting the trajectory into constrained and unconstrained arc segments, thereby enabling the explicit calculation of the state transition matrix at the entrance to the path constraint. Note that since the state transition matrix is computed from the physical vehicle trajectory, all quantities in Eqs. (12) and (13) are associated with the physical vehicle.

$$R = h - x_{\text{physical}}(t_1) \tan 45^o - y_{\text{physical}}(t_1) \tag{12}$$

$$\nabla \mathbf{D} = \left(\frac{\partial R}{\partial \mathbf{x_{physical}}(t_1)} \right)^T \phi(t_0, t_1) \tag{13}$$

Note that since the dispersion gradient is in the direction of maximum violation of the path constraint, the shadow vehicle is initialized in this direction resulting in an addition shown in Eq. (14) in place of the original subtraction in Eq. (7). It is important to note that contributions from multiple dispersions would likely provide a worst case scenario associated with potential violation of the path constraint. As such, shadow vehicles associated with path constraints must incorporate all dispersions associated with the design problem. However, it is unlikely that all dispersions will simultaneously be at the worst case values. To provide an appropriate level of robustness to the path constraint, the combined set of dispersions are constrained to be at the aggregated worst case values. As such, the k^{th} initial state of the shadow vehicle is calculated in a manner similar to Eq. (7), except that the dispersion gradient direction is weighted with the dispersion magnitudes, Δ, as shown in Eq. (14), where N is the number of states of the physical vehicle. This approach ensures that the mixed units associated with the wide range of dispersions are properly

incorporated into a single, worst case displacement direction of the shadow vehicle.

$$\mathbf{x_{0,shadow,k}} = \mathbf{x_{0,physical,k}} + \left(\frac{\nabla \mathbf{D_k} \cdot \mathbf{\Delta_k}}{\sqrt{\sum_{j=1}^{N} (\nabla \mathbf{D_j} \cdot \mathbf{\Delta_j})^2}} \right) \cdot \mathbf{\Delta_k} \tag{14}$$

II.A.5. Monte Carlo Validation

To illustrate the quality of the robust solution that also minimizes the travel time, comparisons are made to a Monte Carlo of the initial velocity uncertainty. Each dispersed trajectory is propagated by interpolating the control history created by the indirect optimization framework. A Gaussian distribution of the dispersed initial velocity is assumed with a 3σ value of 0.9 m/s. The 3σ value is considered the worst case scenario of interest to the designer and is consistent with the initial state displacement of the shadow vehicles. As shown in Figs. 12 and 13, the terminal errors are quite small across the range of initial velocity uncertainties. Of the three trajectories that exceed the 3σ initial velocity uncertainty, only the two high initial velocity trajectories violate the path constraint. As such, the dispersed performance of the robust solution captures the designer's balance between performance (minimum time) and robustness to the path constraint and x_f errors.

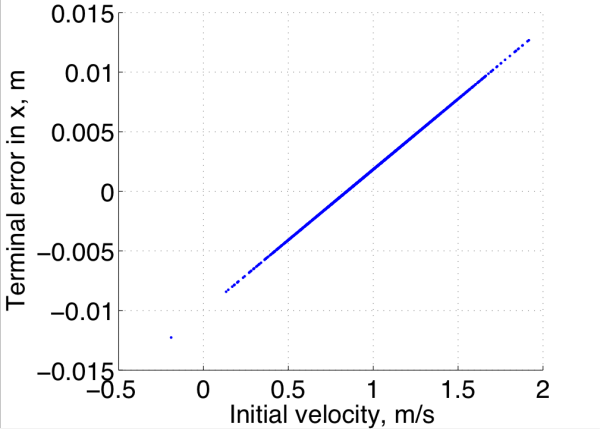

Figure 12: Terminal errors across a range of initial velocities.

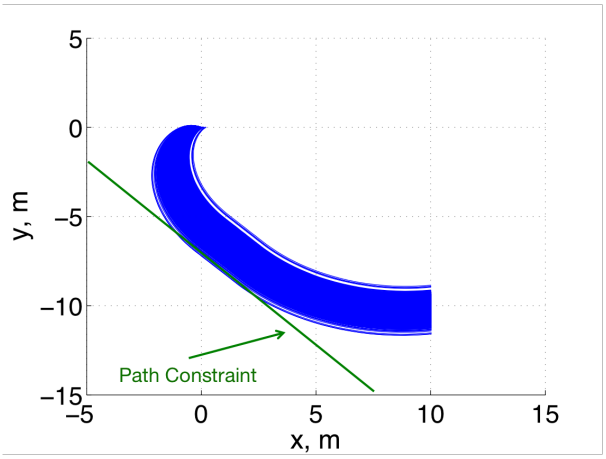

Figure 13: Monte Carlo trajectories associated with initial velocity uncertainty.

III. Robust Hypersonic Mission Design

The robust design methodology described in the prior section is applied to hypersonic mission design. The use of indirect methods enables the creation of high quality solutions that capture the coupled interactions between nominal vehicle performance and robustness considerations to support conceptual design. As such, considerations to dispersed vehicle performance (often neglected during the initial phases of conceptual design) can be captured to provide a more informed conceptual design analysis. For illustrative purposes and consistent with many conceptual hypersonic studies, this investigation assumes planar hypersonic motion in an exponential atmosphere with equations of motion shown in Eqs. (15) - (18). An example with a single dispersion is first presented to illustrate the high quality trajectory shaping made possible by the indirect optimization framework. A second example is then used to illustrate robust design in the presence of multiple dispersions and robustness considerations.

$$\dot{r} = v \sin\gamma \tag{15}$$

$$\dot{\theta} = \frac{v \cos\gamma}{r} \tag{16}$$

$$\dot{v} = -\frac{D}{m} - \frac{\mu \sin\gamma}{r^2} \tag{17}$$

$$\dot{\gamma} = \frac{L}{mv} - \frac{\mu \cos\gamma}{vr^2} + \frac{v\cos\gamma}{r} \tag{18}$$

In the following examples, the angle of attack of a high L/D, high ballistic coefficient vehicle is nominally optimized to maximize terminal velocity at a target downrange as shown by the minimizing cost functional in Eq. (19). The initial and terminal states are specified in Table 1, where the radius of the Earth, R_E, is chosen to be 6378 km. Without consideration to dispersions, the optimal trajectory created via continuation using the indirect methodology is shown in Figs. 14 and 15. The corresponding optimal flight path angle history and angle of attack profile are shown in Figs. 16 and 17. As expected, the vehicle phugoids at high altitudes in order to minimize drag during the downrange flight. During the terminal portion of the trajectory, the vehicle dives to maximize velocity on target.

Table 1: Initial and terminal conditions.

Parameter	Initial Value	Terminal Value
r	$R_E + 40$ km	$R_E + 0$ km
V	2 km/s	free
γ	-10 deg	free
θ	0 deg	4.5 deg

$$J = -v_f^2 \tag{19}$$

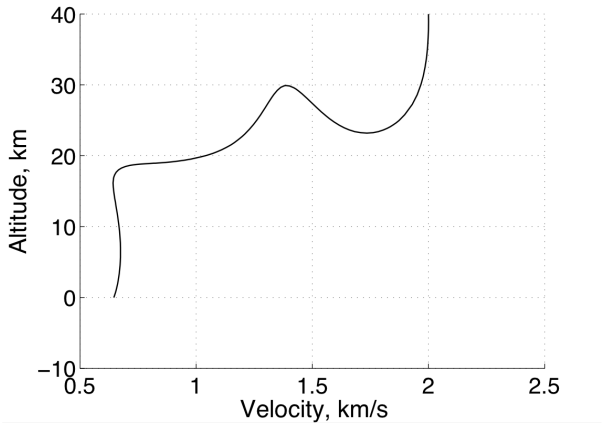

Figure 14: Altitude vs. velocity for maximum velocity trajectory.

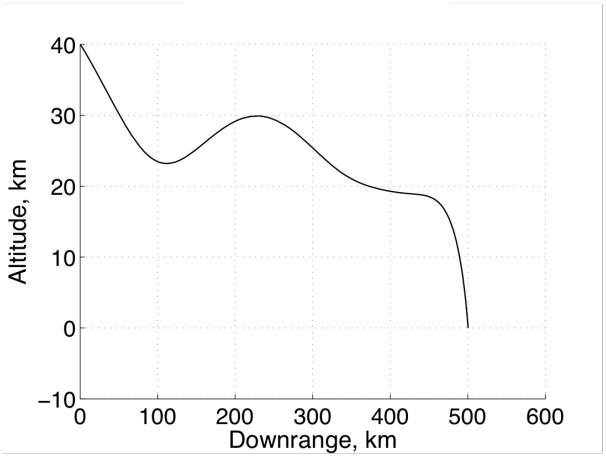

Figure 15: Altitude vs. downrange for maximum velocity trajectory.

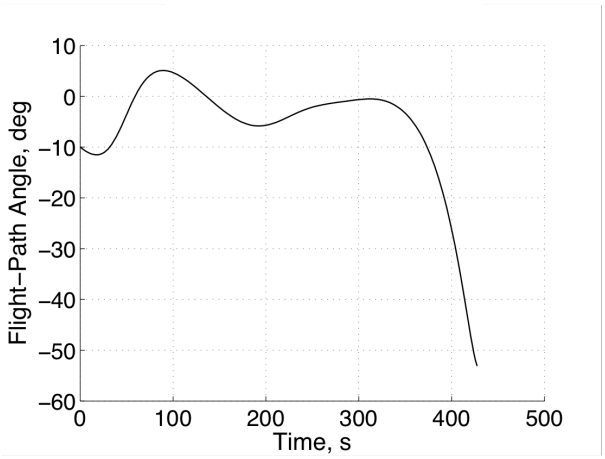

Figure 16: Flight-path angle vs. time for maximum velocity trajectory.

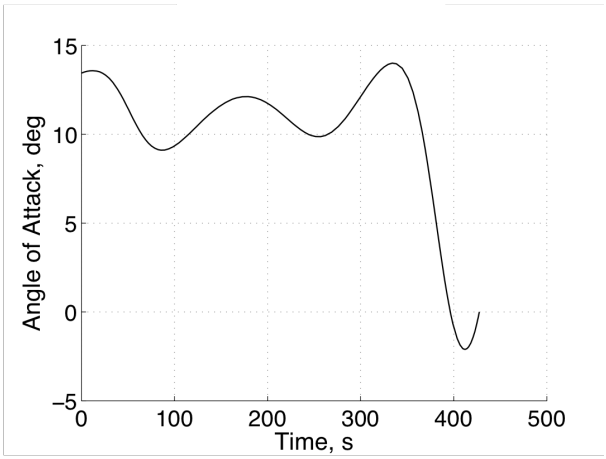

Figure 17: Angle of attack vs. time for maximum velocity trajectory.

III.A. Planar Hypersonic Flight with a Single Dispersion

This trajectory is consistent with the initial vehicle performance assessments common to early conceptual design. While this solution provides insight into vehicle capability, it does not consider robustness considerations that may also eventually be of interest to the designer. For example, the designer may also be interested in creating a trajectory that is robust to terminal downrange dispersions. For illustrative purposes, a single dispersion in flight path angle with a maximum error of two degrees is considered. Without including this dispersion in the design process, the shadow vehicle would result in a large downrange error as shown in Fig. 18. To create a robust terminal downrange trajectory due to initial flight path angle dispersions, a robustness metric is created as shown in Eq. (20). When minimizing the robustness metric, a robust trajectory is created as shown in Fig. 19. Note that the comparison between the physical and shadow vehicle occurs at the same final time. While the physical vehicle is constrained to terminate at the ground, the shadow vehicle is free to terminate at any terminal state (which occurs slightly below the ground for this example). However, the methodology does create a robust terminal downrange solution due to errors in initial flight path angle. In fact, the physical and shadow vehicle trajectories converge well before the ground is reached.

$$R = (\theta_{f,\text{physical}} - \theta_{f,\text{shadow}})^2 \tag{20}$$

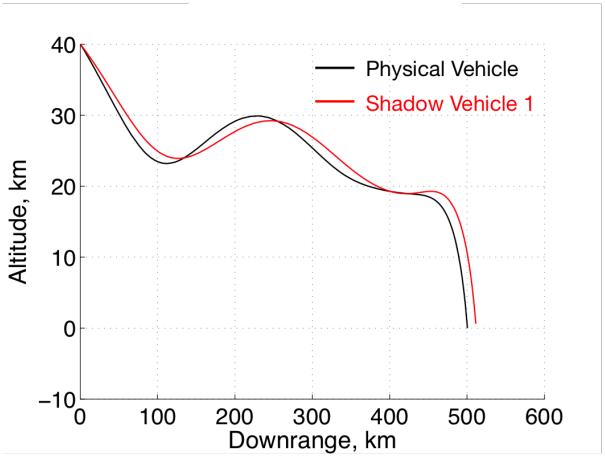

Figure 18: Maximum velocity trajectory with propagated worst case dispersion in flight-path angle.

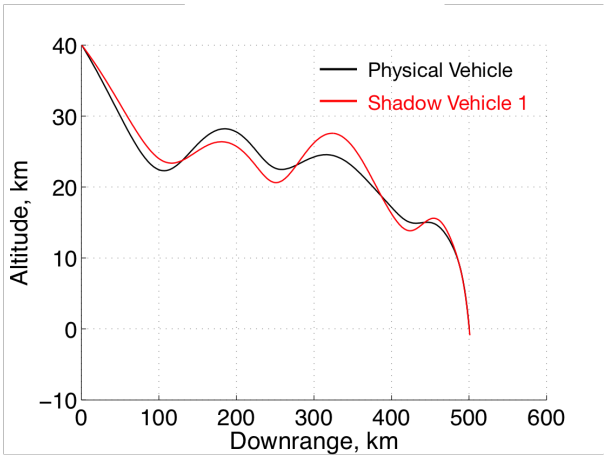

Figure 19: Robust downrange trajectory with propagated worst case dispersion in flight-path angle.

Figs. 20 - 23 illustrate the change in trajectories as the designer preference is altered from nominal performance (terminal velocity) to robust performance (small terminal downrange errors). Note that in all cases, the optimal trade in nominal and robust performance is captured by the weighted objective functional shown in Eq. (21). As such, the designer is able to identify sufficiently robust trajectories that also maximize velocity on target. As shown, the robust trajectories illustrate significant deviations from the nominal solution. In general, the overall phugoiding structure and angle of attack profile is substantially altered. The ability to incorporate robust design considerations early in the conceptual design process can provide a substantially different perspective of the overall hypersonic flight profile.

$$J = w(-v_f^2) + (1-w)(\theta_{f,\text{physical}} - \theta_{f,\text{shadow}})^2 \tag{21}$$

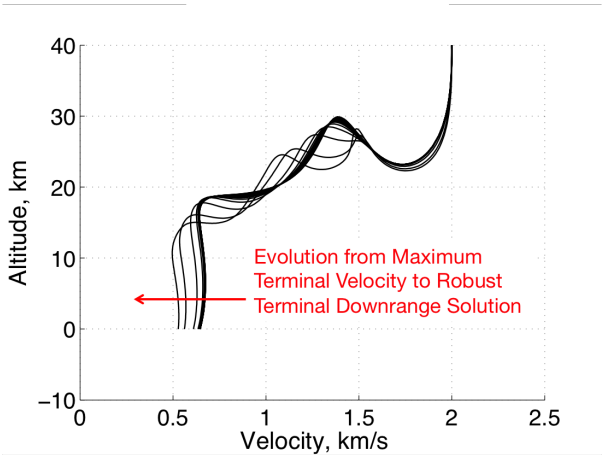

Figure 20: Altitude vs. velocity evolution due to transition from nominal to robust performance.

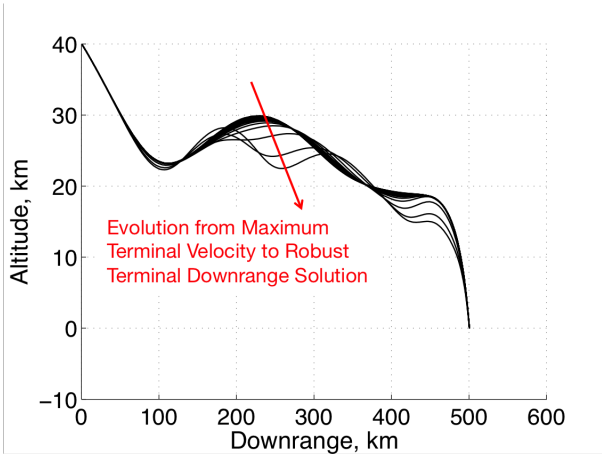

Figure 21: Altitude vs. downrange evolution due to transition from nominal to robust performance.

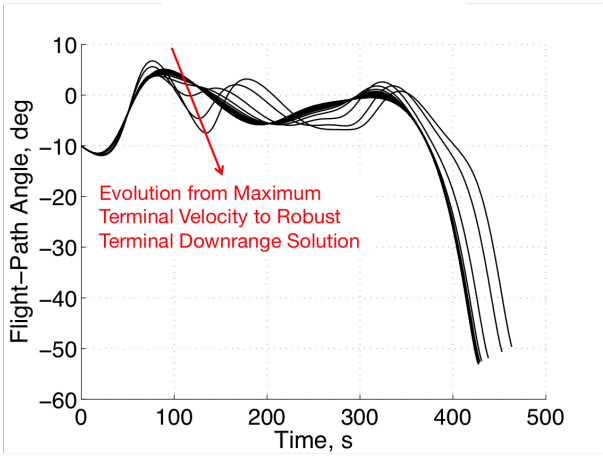

Figure 22: Flight-path angle vs. time evolution due to transition from nominal to robust performance.

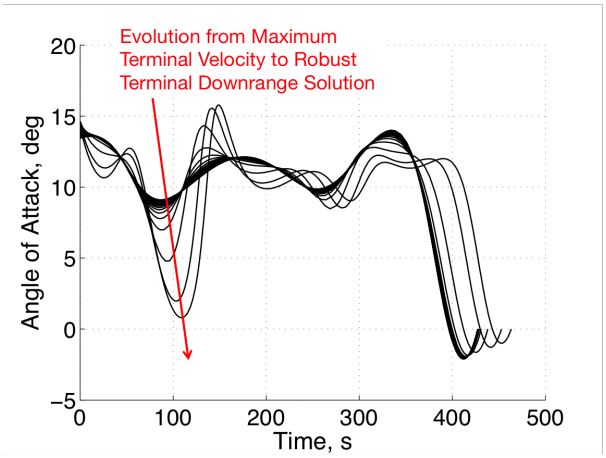

Figure 23: Angle of attack vs. time evolution due to transition from nominal to robust performance.

This additional insight during the conceptual design process enables the creation of optimal trades of nominal performance to robust design considerations. In this example, the optimal trade in maximum terminal downrange error vs. nominal terminal velocity can be rapidly created using the solutions shown in Figs. 20 - 23. As such, the optimal trade in nominal performance (terminal velocity) and robust design (terminal downrange error) can be created as shown in Fig. 24.

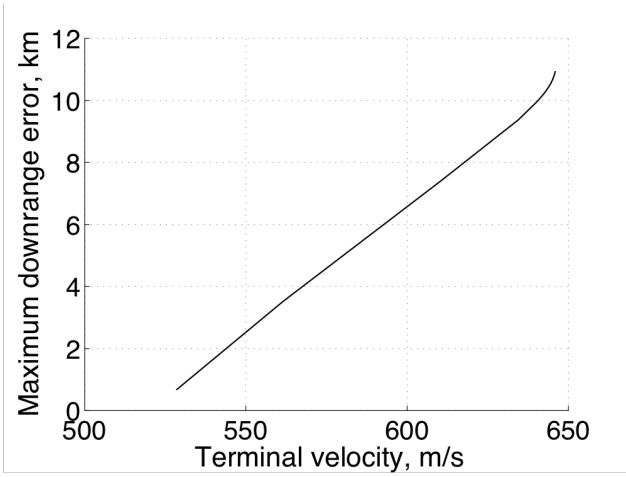

Figure 24: Pareto frontier of downrange error vs. terminal velocity.

III.B. Planar Hypersonic Flight with Multiple Dispersions and A Path Constraint

As illustrated with the Brachistochrone example described in Section II.A, multiple dispersions can be addressed using multiple shadow vehicles. In the following example, a 3σ robust hypersonic trajectory is created due to the presence of select dispersions (for illustrative purposes) shown in Table 2 where the minimizing objective functional shown in Eq. (22) is used. The weighting, w, trades performance (terminal velocity) with the aggregated robustness (terminal downrange error) across all M shadow vehicles. Robustness to parameters, such as atmospheric and aerodynamic scaling parameters, can be easily performed by treating each parameter, p, as a state with a time derivative of zero as shown in Eq. (23). When performing robust design to all dispersions as shown in Fig. 25, it is clear that the shadow vehicles result in notable downrange errors, with the shadow vehicles corresponding to dispersions in C_L (Shadow Vehicle #4) and in C_D (Shadow Vehicle #5) dominating. Since the downrange errors from these two cases dominate, the robust design solver is heavily weighted toward these dispersions. The fact that no robust solution can be found implies that the downrange error from aerodynamic dispersions cannot be substantially reduced. This is further verified by performing robust design with consideration to C_L uncertainties only. As shown by the best robust solution in Fig. 26, it is not possible to substantially reduce the downrange errors associated with this uncertainty. This is reasonable considering the particular flight profile analyzed. To provide robust solutions with respect to aerodynamics, the vehicle would be required to reduce its interaction with the atmosphere. However, to maximize velocity at the target, the vehicle phugoids during the majority of flight and dives after reaching the target. As such, the flight profile already substantially limits the vehicle's interaction with the atmosphere in order to maximize velocity on target, preventing the creation of robust solutions with respect to aerodynamic uncertainties.

Table 2: Hypersonic trajectory dispersions (all assumed Gaussian for illustration).

Parameter	3σ *Value*	Shadow #
Initial flight-path angle, γ_0	2 deg	Vehicle 1
Initial altitude, r_0	3 km	Vehicle 2
Atmospheric density multiplier	0.2	Vehicle 3
C_L multiplier	0.1	Vehicle 4
C_D multiplier	0.1	Vehicle 5

$$J = w(-v_f^2) + (1-w)\left(\sum_{i=1}^{M}(\theta_{f,\text{physical}} - \theta_{f,\text{shadow},i})^2\right) \tag{22}$$

$$\dot{p} = 0 \tag{23}$$

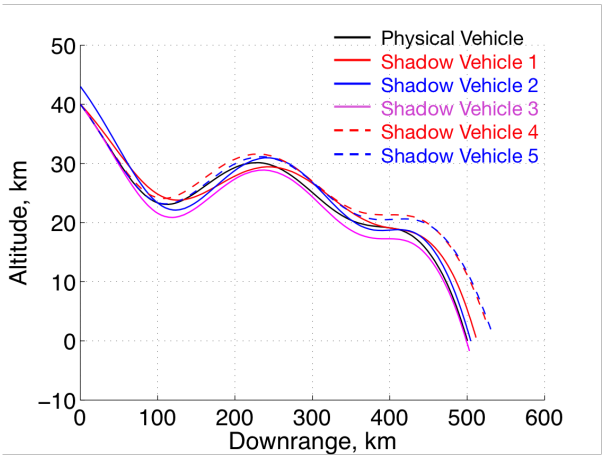

Figure 25: Altitude vs. downrange for all dispersions.

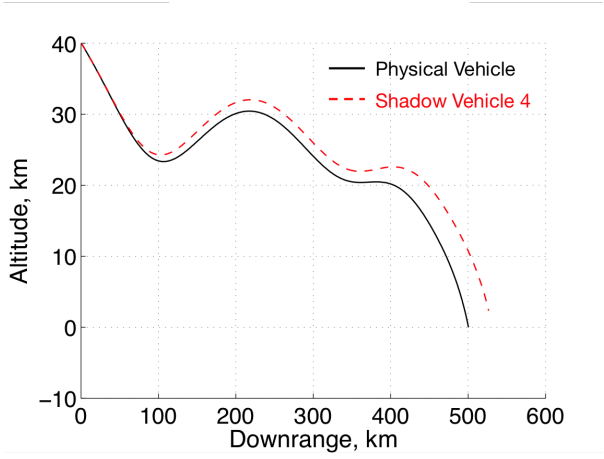

Figure 26: Altitude vs. downrange due to C_L uncertainty only.

After removing the aerodynamic uncertainties, it is clear from Figs. 28 and 29 that a highly robust solution can be found that appropriately accommodates the remaining relevant dispersions. Note that the robust solution is able to accommodate a wide range of shadow vehicle trajectories in a manner that ensures all terminate at the target downrange. The angle of attack profile shown in Fig. 27 is created by coupling the states and costates of the physical and three shadow vehicles in an explicit manner as described by Eq. (10) in Section II.A.3. This explicit mathematical relationship of all of the vehicles within the optimal control expression enables the detailed creation of such complex control histories that provide the best possible combined nominal and robust performance.

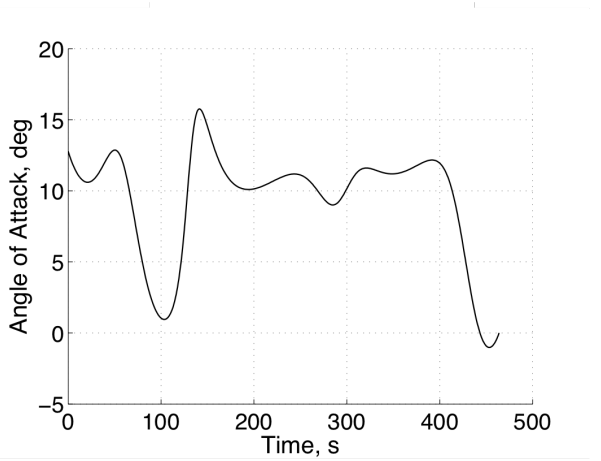

Figure 27: Angle of attack vs. time for robust trajectory without aerodynamic dispersions.

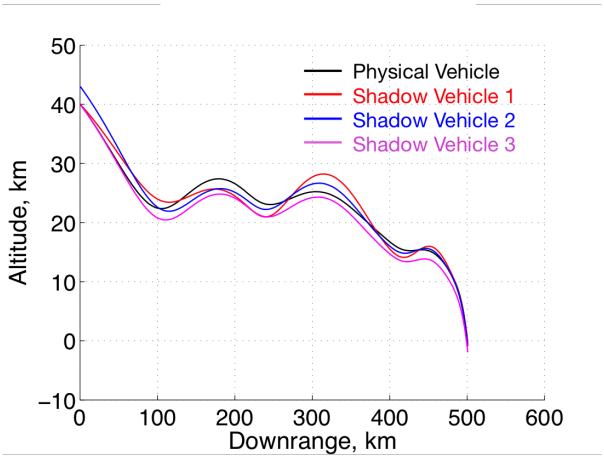

Figure 28: Altitude vs. downrange for non-aerodynamic dispersions.

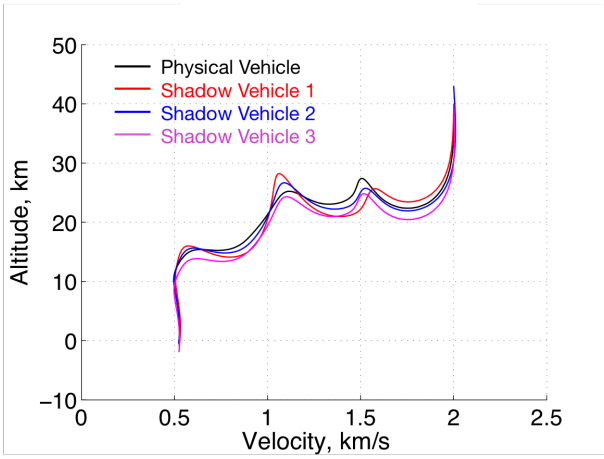

Figure 29: Altitude vs. velocity for non-aerodynamic dispersions.

For validation, a 2000 case Monte Carlo is performed with the dispersed results shown in Figs. 30 and 31. As expected, all of the terminal state dispersions are quite small while the maximum terminal velocity is retained as best as possible. For comparison, the histogram of the dispersed performance of the nominal maximum velocity solution is also shown in Fig. 30. As expected, the robust solution provides a substantial improvement in terminal downrange error. Note that this example highlights an important consideration discussed in Section I. While the initial uncertainties may be assumed to be Gaussian, these dispersions do not necessarily correspond to Gaussian dispersions at future times, and this result is evident by the skewed distribution of the robust trajectories shown in Fig. 30. The use of shadow vehicles enables the worst case dispersions to be captured without the need to consider the form of distributions or calculation of statistical moments throughout the trajectory. Finally, it is important to note that while the robust physical vehicle trajectory was designed to ensure that all shadow vehicles converge to the terminal point, this does not mean that all dispersed trajectories have a near zero terminal downrange error. This is evident in the robust solutions shown in Fig. 30. While it is impossible to ensure that every dispersed trajectory has a near zero terminal downrange error, the use of shadow vehicles to independently assess various worst case dispersions provides an efficient orthogonal set of cases to use in the robust design framework. In fact, the entire design process (including formulation of necessary conditions of optimality, etc.) was accomplished in approximately 30 minutes using a single 2.6 GHz processor.

As a final example, the designer may also require the trajectory to be robust to a particular heat rate constraint. To account for the heat rate constraint, an additional shadow vehicle is included that accounts

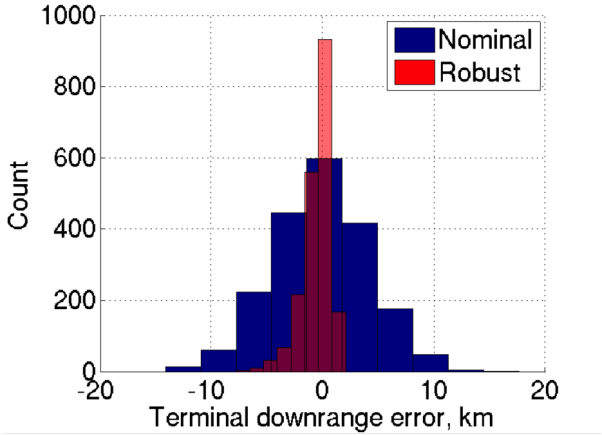

Figure 30: Histogram of dispersed performance using nominal and robust trajectory control profiles.

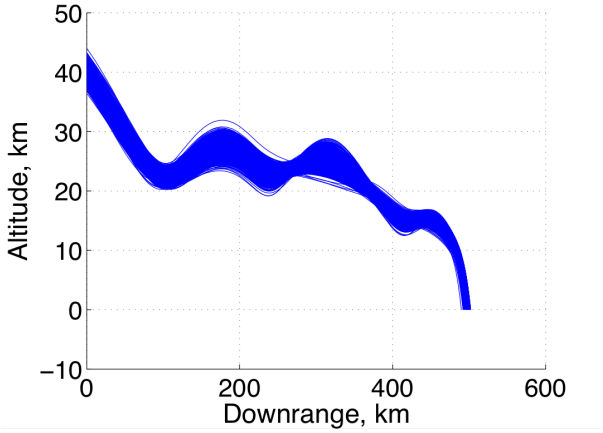

Figure 31: Altitude vs. downrange for robust trajectory control profile.

for the worst case scenario as described in Section II.A.4. This additional consideration results in the construction of a physical trajectory with a sufficient push-off factor from the heat rate constraint as shown in Fig. 32. As shown in Fig. 33, the need for a sufficient push-off factor from the heat rate constraint requires the physical vehicle to phugoid at higher altitudes. This result directly contrasts the trend in robust trajectories to initially dive deeper into the atmosphere as shown in Fig. 21. As such, the ability to construct trajectories that are also robust to terminal downrange errors is severely limited, and this limitation can be easily observed by the relatively large downrange errors of the shadow vehicles also shown in Fig. 33. The dispersed Monte Carlo performance of the robust trajectory solutions with and without the heat rate constraint is shown in Fig. 34, illustrating the noticeable degradation in terminal downrange accuracy due to the accommodation of the heat rate constraint. Fig. 35 illustrates that the constructed control profile is indeed robust to the heat rate constraint.

The construction of the robust solution was accomplished in approximately 45 minutes on a 2.6 GHz processor. This is particularly fast considering the numerous dispersions captured by the shadow vehicles and sensitivities about the physical vehicle trajectory captured by the state transition matrix that are also included in the optimization process. As such, this example consists of 50 states and 50 costates with over 100 boundary conditions that are simultaneously satisfied within the indirect optimization framework. The automation described in Section I enables the creation of and solution to such large indirect optimization problems. It is expected that the natural parallelization of the indirect optimization framework will enable even larger systems to be assessed in a fraction of the time.[15]

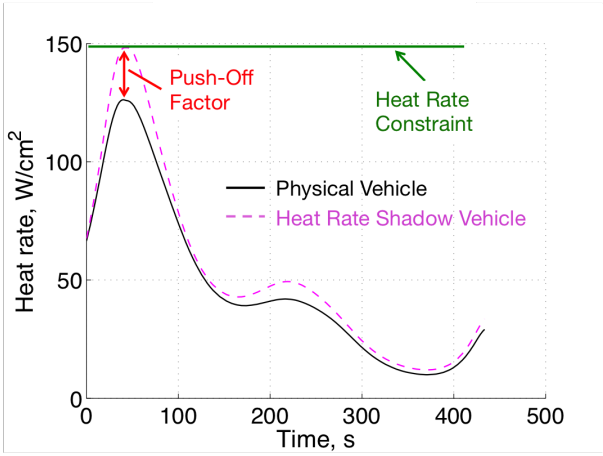

Figure 32: Physical trajectory with sufficient push-off from heat rate constraint.

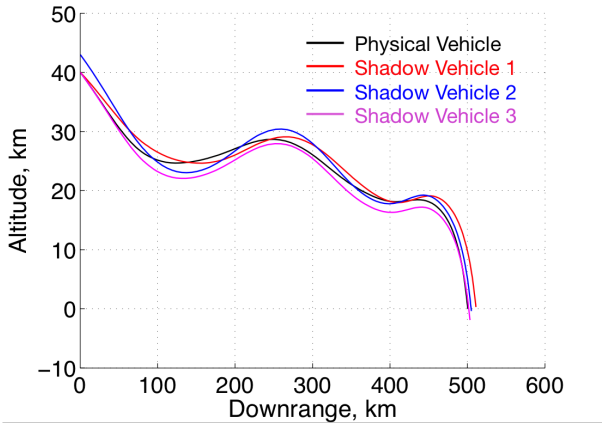

Figure 33: Altitude vs. downrange for trajectories with robustness to heat rate constraint.

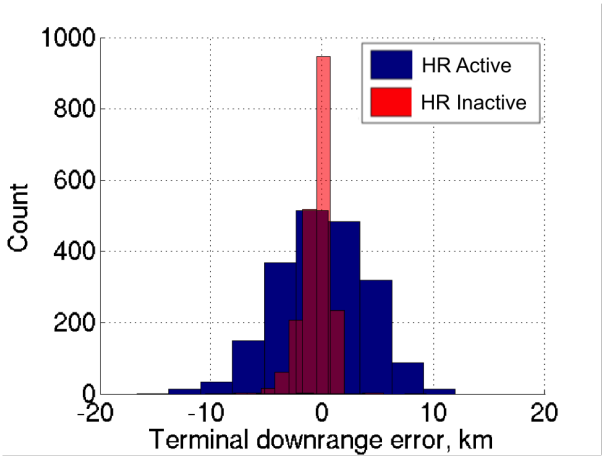

Figure 34: Histogram of dispersed performance of robust trajectories with and without heat rate constraint.

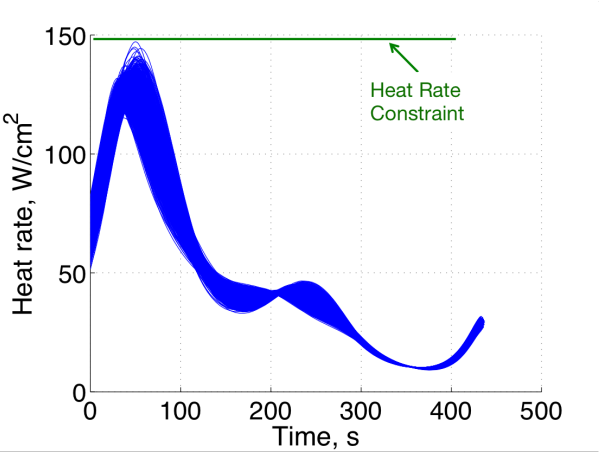

Figure 35: Heat rate vs. time for dispersed trajectories robust to heat rate constraint.

IV. Conclusions

This investigation illustrates that robust trajectory design can be efficiently performed using an indirect optimization framework. The use of shadow vehicles enables the worst case dispersions to be captured and propagated throughout the trajectory without the need to propagate moments or to assume a form of the distributions throughout the trajectory. By propagating the shadow vehicles with the same control history as the physical (nominal) vehicle, an explicit relationship can be created for the optimal control solution that is a function of the states and costates of the physical and shadow vehicles. This deep mathematical coupling enables the creation of high quality robust solutions that efficiently capture the worst case dispersions that is generally of most interest to the designer. By dynamically constraining the initial states of the shadow vehicles to reside in the worst case direction from the physical vehicle, the trajectory of the physical vehicle can be modified during the design process to construct robust solutions. This direction is calculated by using a state transition matrix along the physical vehicle trajectory. The corresponding sensitivities along this central trajectory are used to calculate the worst case dispersion direction for each individual shadow vehicle.

Since the state transition matrix elements are added as states to the indirect optimization framework, there is a large initial growth in the dimension of the two-point boundary value problem. As each new dispersion is considered, a corresponding shadow vehicle must be added, resulting in only a linear growth in the number of states as dispersions are included. Ultimately, a system of approximately 100 states and costates is created for the planar hypersonic problem. The ability to construct the necessary conditions of optimality automatically using Mathematica and to solve complex indirect optimization problems using continuation removes much of the burden associated with formulating and solving the corresponding boundary value problem.

By formulating a weighted objective functional that trades performance and robustness considerations of interest to the designer, high quality robust solutions are created for a simple Brachistochrone problem and for a planar hypersonic example. The performance of the robust solutions is evaluated using Monte Carlo analyses. The narrow distributions about the desired robust quantities illustrate the quality of robust solutions created by the indirect optimization framework. While the example trajectories only consist of a small number of dispersions for illustrative purposes, the overall robust trajectory design methodology can be extended to an arbitrary number of states and dispersions. As a result, this robust design methodology is capable of explicitly capturing the considerations of most interest to conceptual hypersonic trajectory designers while simultaneously leveraging all of the available mathematical information that relates nominal trajectory performance to robust design considerations.

Acknowledgements

Approved for Public Release. Distribution Unlimited. Case Number 88ABW-2015-2599.

References

[1]Fahroo, F. and Ross, I. M., "Direct Trajectory Optimization by a Chebyshev Pseudospectral Method," *Journal of Guidance, Control, and Dynamics*, Vol. 25, No. 1, 2002.

[2]Betts, J. T., *Practical Methods for Optimal Control and Estimation Using Nonlinear Programming (Second Edition)*, SIAM, Philadelphia, PA, Nov. 2010.

[3]Fahroo, F., Doman, D. B., and Ngo, A. D., "Modeling Issues in Footprint Generation for Reusable Launch Vehicles," *2003 IEEE Aerospace*, IEEE, March 2003, pp. 2791–2799.

[4]Jorris, T., Schulz, C., Friedl, F., and Rao, A., "Constrained Trajectory Optimization Using Pseudospectral Methods," *AIAA Atmospheric Flight Mechanics Conference and Exhibit*, AIAA 2008-6218, Honolulu, HI, Aug. 2008.

[5]Jorris, T. R. and Cobb, R. G., "Three-Dimensional Trajectory Optimization Satisfying Waypoint and No-Fly Zone Constraints," *Journal of Guidance, Control, and Dynamics*, Vol. 32, No. 2, March 2009, pp. 551–572.

[6]Josselyn, S. and Ross, I. M., "Rapid Verification Method for the Trajectory Optimization of Reentry Vehicles," *Journal of Guidance, Control, and Dynamics*, Vol. 26, No. 3, May 2003, pp. 505–508.

[7]Grant, M. J. and Braun, R. D., "Rapid Indirect Trajectory Optimization for Conceptual Design of Hypersonic Missions," *Journal of Spacecraft and Rockets*, Vol. 52, No. 1, Jan. 2015, pp. 177–182.

[8]Grant, M., *Rapid Simultaneous Hypersonic Aerodynamic and Trajectory Optimization for Conceptual Design*, Ph.D. thesis, Georgia Institute of Technology.

[9]Small, T. V., *Optimal Trajectory-Shaping with Sensitivity and Covariance Techniques*, MS Thesis, Massachusetts Institute of Technology, May 2010.

[10]Saunders, B. R., *Optimal Trajectory Design Under Uncertainty*, MS Thesis, Massachusetts Institute of Technology, June 2012.

[11]Prabhakar, A., Fisher, J., , and Bhattacharya, R., "Polynomial Chaos-Based Analysis of Probabilistic Uncertainty in Hypersonic Flight Dynamics," *Journal of Guidance, Control, and Dynamics*, Vol. 33, No. 1, 2010.

[12]Grant, M. J. and Mendeck, G. F., "Mars Science Laboratory Entry Optimization Using Particle Swarm Methodology," AIAA 2007-6393, *AIAA Atmospheric Flight Mechanics Conference and Exhibit*, Hilton Head, SC, 20-23 Aug. 2007.

[13]Mendeck, G. F. and Carman, G. L., "Guidance Design for Mars Smart Landers Using The Entry Terminal Point Controller," AIAA-2002-4502, *AIAA Atmospheric Flight Mechanics Conference and Exhibit*, Monterey, CA, 5-8 Aug. 2002.

[14]Bryson, A. E. and Ho, Y.-C., *Applied Optimal Control*, Taylor and Francis, 1975.

[15]Antony, T., *Rapid Indirect Trajectory Optimization on Highly Parallel Computing Architectures*, MS Thesis, Purdue University, Dec. 2012.